Large Eddy Simulation of Crashback in Marine Propellers

Martin Vyšohlíd* and Krishnan Mahesh†
University of Minnesota, Minneapolis, MN 55455

The large eddy simulation methodology is applied to predict the flow around a marine propeller in the forward and crashback modes of operation. A non-dissipative, robust numerical algorithm developed by Mahesh et al. (2004, J. Comput. Phys., 197: 215-240) for unstructured grids was extended to include the effect of rotating frame of reference. The thrust and torque coefficients, circumferentially averaged mean velocity and root mean square fluctuation of velocity obtained from the simulation are compared to experimental data and good agreement is observed. The crashback simulations show the presence of a highly unsteady ring-vortex, and irregular low frequency unsteady loads on the propeller.

I. Introduction

CRASHBACK is an extreme operating condition for marine propulsors that often determines propulsor strength, and strongly affects overall maneuverability. Figure 1 defines four different modes of propeller operation based on the sense of the propeller rotation and the direction of the relative velocity of far field flow with respect to the propeller. Crashback is seen to be the operating condition where the propeller rotates in the reverse direction while the vessel moves in the forward direction. The flow around the propeller during crashback is characterized by massive separation, and large-scale unsteadiness. A prominent feature of the flow is an unsteady ring-vortex in the vicinity of the propeller disk. Jiang et al.[1] performed experiments of propeller crashback which provide PIV data on the ring-vortex, and suggest that the unsteadiness of the ring-vortex is related to the forces experienced by the propeller. Detailed experiments which measure flow velocity in crashback using PIV and LDV were recently performed by Jessup et al.[2]

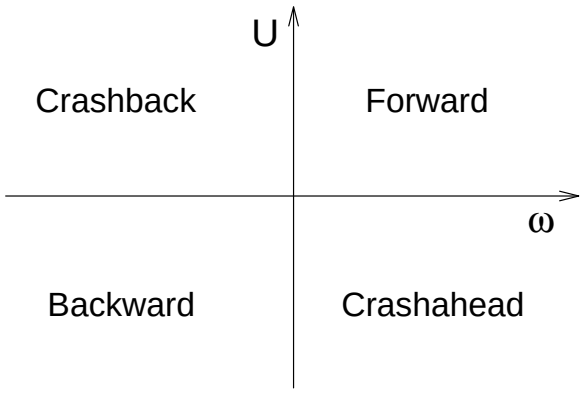

Figure 1: Classification of propeller operation based on the direction of angular velocity ω of the propeller and the direction of the free-stream velocity *U*.

* Graduate Research Assistant, Aerospace Engineering & Mechanics, AIAA student member
† Associate Professor, Aerospace Engineering & Mechanics, AIAA member

The unsteady Reynolds-averaged Navier-Stokes equations (RANS) represent the state-of-the-art in computational prediction of the viscous flow around propellers[3–5]. Currently, RANS appears capable of predicting forward mode and backing; however, significant disagreement with data is observed in crashback and crashahead conditions. For example, Chen & Stern[3] show that RANS is within 5% of experimental data for thrust and torque in the forward mode and within 6.5% when backing, but crashback or crashahead increases the error to 110%. Also the computed results showed only 3% oscillation about the mean while the experiment showed 20%.

It is likely that RANS is unable to adequately predict crashback because of the pervasive large-scale unsteadiness. This paper therefore uses the large-eddy simulation methodology to simulate propeller crashback. LES is a three-dimensional and unsteady computational approach where the Navier-Stokes equations are spatially filtered, and the resolved scales of motion are directly computed while the effect of the unresolved scales is modeled. A known limitation of LES (without wall models) is the near-wall resolution requirements for external flows at high Reynolds numbers. It is hoped that the near-wall resolution is not as critical for the crashback problem which has massive geometry-induced separation. This assumption will be tested by comparison to experimental data.

The paper is organized as follows. Section II.A briefly describes the governing equations and numerical method. The propeller geometry and computational grid are outlined in section II.B. Some results from the computations are shown in section III. Two cases are considered: one in the forward mode (III.A) and one in the crashback mode of operation (section III.B), respectively. A brief summary in section IV concludes the paper.

II. Simulation details

A. Numerical method

The simulations are performed in a frame of reference that rotates with the propeller. The incompressible Navier-Stokes equations are solved in a rotating coordinate system. The governing equations in a rotating frame can either be written for the velocities measured in a stationary frame or for velocities measured in the rotating frame. The form of the governing equations may be strongly conservative[6] or in a form where system rotation produces a source term.[7] This paper uses the following form of the governing equations:

$$\frac{\partial u_i}{\partial t} + \frac{\partial}{\partial x_j}\left(u_i u_j - u_i \varepsilon_{jkl}\omega_k x_l\right) = -\frac{\partial p}{\partial x_i} - \varepsilon_{ijk}\omega_j u_k + \nu \frac{\partial^2 u_i}{\partial x_j \partial x_j},$$

$$\frac{\partial u_i}{\partial x_i} = 0.$$

Here u_i is the inertial velocity, p is the pressure, x_i are coordinates in the rotating frame, t is time, ω_i is the angular velocity of the rotating frame of reference, and ν is the kinematic viscosity. Note that the density is absorbed in pressure. Also, the Einstein summation convention is used and ε_{ijk} denotes the permutation symbol.

The LES equations are obtained by spatially filtering (denoted by overbar) the Navier-Stokes equations. The filter is assumed to commute with the spatial and temporal derivatives. Applying the filter and using the approximation

$$\overline{u_i \varepsilon_{jkl}\omega_k x_l} \approx \overline{u}_i \varepsilon_{jkl}\omega_k x_l,$$

we get

$$\frac{\partial \overline{u}_i}{\partial t} + \frac{\partial}{\partial x_j}\left(\overline{u}_i \overline{u}_j - \overline{u}_i \varepsilon_{jkl}\omega_k x_l\right) = -\frac{\partial \overline{p}}{\partial x_i} - \varepsilon_{ijk}\omega_j \overline{u}_k + \nu \frac{\partial^2 \overline{u}_i}{\partial x_j \partial x_j} - \frac{\partial \tau_{ij}}{\partial x_j},$$

$$\frac{\partial \overline{u}_i}{\partial x_i} = 0$$

where

$$\tau_{ij} = \overline{u_i u_j} - \overline{u}_i \overline{u}_j$$

is the subgrid stress and is modeled. The dynamic Smagorinski model as proposed by Germano et al.[8] and modified by Lilly[9] is used to model the subgrid stress.

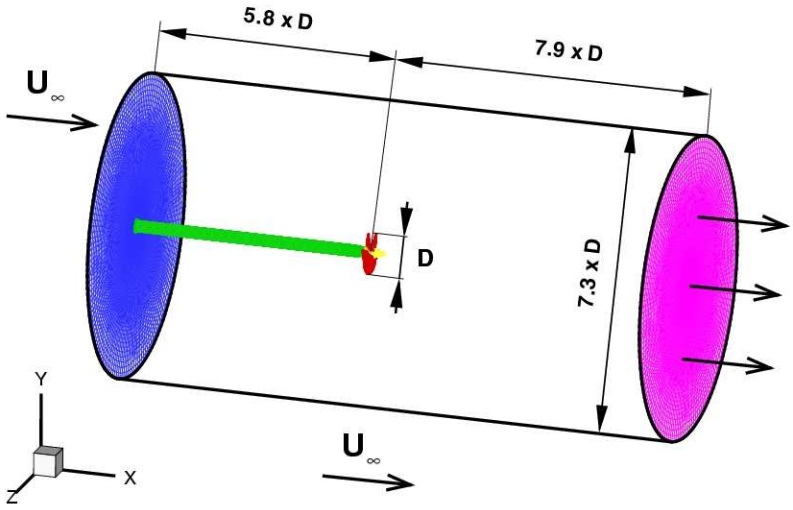

a)

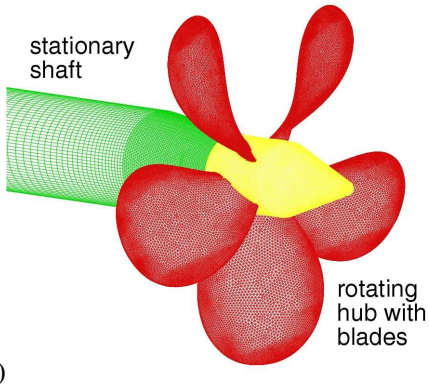

b)

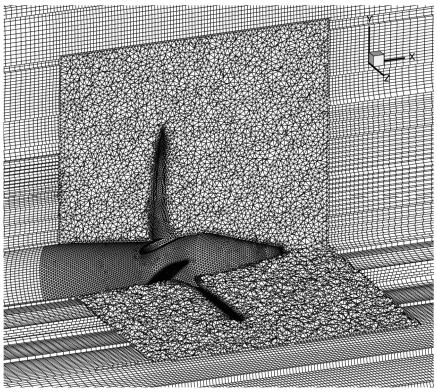

c)

Figure 2: (a) Computational domain, (b) detail view of the propeller (c) mesh in propeller neighborhood.

The above equations are solved using a numerical method developed by Mahesh et al.[10] for incompressible flows on unstructured grids. The algorithm is derived to be robust without numerical dissipation. It is a finite-volume approach which stores the Cartesian velocities and the pressure at the centroids of the cells (control volumes) and the face normal velocities are stored independently at the centroids of the faces. A predictor-corrector approach is used. The predicted velocities at the control volume centroids are first obtained and then interpolated to obtain the face-normal velocities. The predicted face normal velocity is projected so that continuity is discretely satisfied. This yields a Poisson equation for pressure which is solved iteratively using a multigrid approach. The pressure field is used to update the Cartesian control volume velocities using a least-squares formulation. Time advancement is implicit and is performed using the Crank-Nicholson scheme. The algorithm has been validated for a variety of problems[10] over a range of Reynolds numbers.

B. Propeller geometry and computational grid

The computations were performed for Propeller 4381, which is a five bladed, right-handed propeller with variable pitch, no skew and rake. A detailed description of the geometry may be found in Ref. 2.

Figure 2a shows a schematic of the cylindrical computational domain, whose diameter is 7.3 times the propeller diameter, and length is 13.75 times the propeller diameter. The size of the domain was chosen to match the diameter of the widest part of the water tunnel used in experiments of Jessup et al. A constant free-stream velocity boundary condition is specified at the inlet and lateral boundaries. Convective velocity boundary conditions are prescribed at the outflow. A detail view of the propeller is shown in Fig. 2b. The boundary condition on the propeller, hub and the conical tip are specified using $\mathbf{u} = \omega \times \mathbf{r}$, while the shaft is stationary; i.e. $\mathbf{u} = 0$. All five blades of the propeller are represented in the computation.

A commercial grid generator (Gambit & TGrid, Fluent Corporation) was used for the grid generation. Figure 2c shows the mesh around the propeller. Tetrahedral elements are used in the immediate vicinity of the propeller to match the complicated geometry of the blades, while hexahedral elements and prisms are used farther from the propeller. Four layers of prisms were grown on the surfaces of blades in order to improve the resolution of boundary layers on blades. First, the surface grids were created by Gambit, then the grid was imported into TGrid. The boundary layers on blades were grown in TGrid, then the tetrahedral elements were generated around the propeller and finally the grid was extruded upstream and downstream. The smallest grid size is 1.7×10^{-3} of the propeller diameter, and is found on the edges of the blades; size functions were used to control the growth rate of the grid size to obtain a final mesh with size of approximately 13 million control volumes.

III. Results

A. Forward Operation

Simulations were performed in the forward mode at advance ratio J=0.889 for which thrust and torque were measured in a 36 inch water tunnel by Jessup et al.,[2] and in a tow-tank by Hecker & Remmers[11] and Jessup (private communication). The advance ratio J is defined as $J = U/(nD)$ where U is the free-stream velocity, n is the propeller rotational speed in revolutions per time unit and D is the propeller diameter. The computation was started with uniform flow as the initial condition and with a Reynolds number of 12,000. The Reynolds number is based on the free stream velocity and on the diameter of the propeller. After 6.9 propeller revolutions, the Reynolds number was increased 10 times and after another 2.5 propeller revolutions it was further increased to 894,000 to match the water tunnel experiment. It is shown below that the qualitative features of the flow are captured and that the computed values of thrust and torque show good agreement with experimental measurements in a tow-tank. Also, Reynolds number sensitivity is investigated.

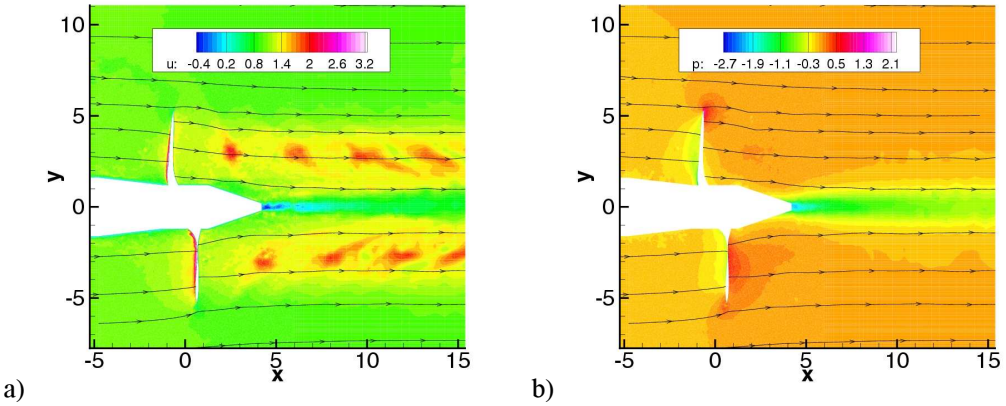

Figure 3: Computed results for forward operation J = 0.889, Re = 894,000: (a) streamlines and contours of velocity normalized by U, (b) streamlines and contours of pressure normalized by ρU^2 .

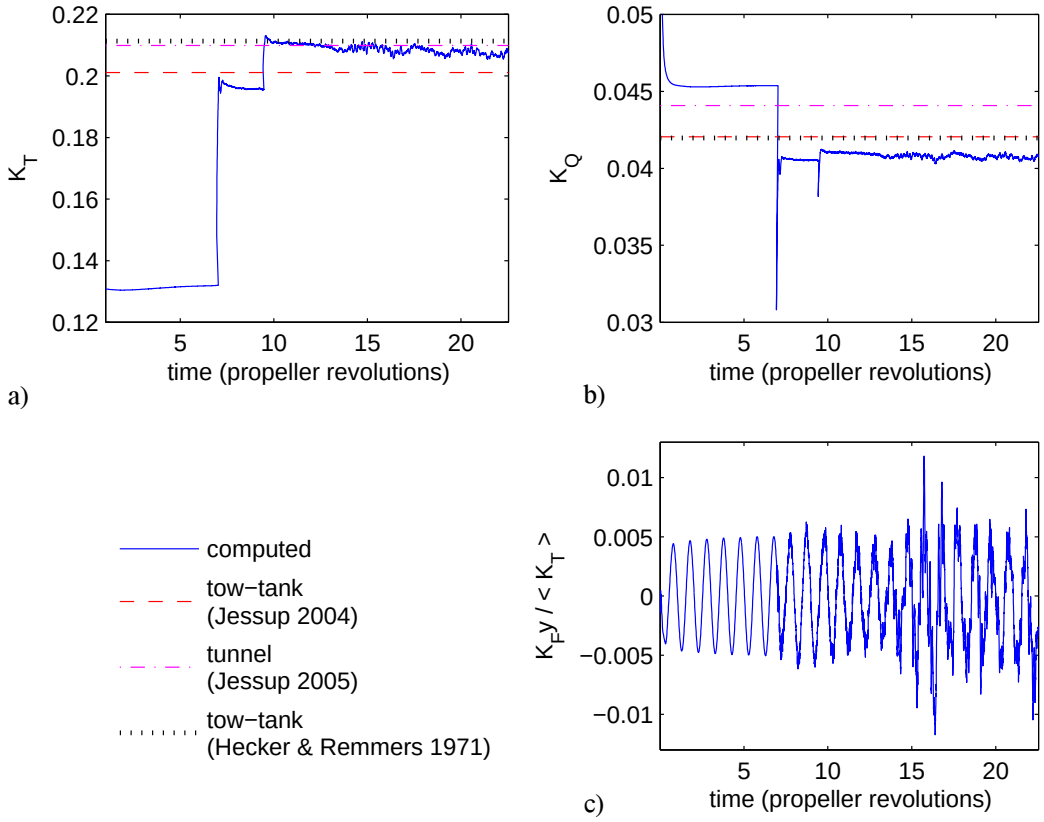

Figure 4: Non-dimensional (a) thrust K_T, (b) torque K_Q and (c) K_F - component of force perpendicular to propeller axis in direction fixed with respect to steady coordinates normalized by average thrust $<K_T>$=0.21 for *J* = 0.889 as they develop during the computation. The computation was started with Reynolds number of 12,000 and then increased in two steps to *Re* = 120,000 and experimental *Re* = 894,000. All experimental data are from Table 1.

Figure 3a shows streamlines and axial velocity contours for the design advance ratio J=0.889 at a Reynolds number of 894,000. Note, that the flow is accelerated as it passes through the propeller. As the flow accelerates, the region defined by the streamlines passing through the propeller region (slipstream) contracts. Patches of higher velocity flow correspond to passage of individual blades. The acceleration of fluid is related to the pressure gradient, which in turn determines the thrust and torque on the propeller. Part of the acceleration occurs upstream of the propeller as the pressure on upstream (suction) side of the blade is lower than the ambient pressure, and part of the acceleration occurs downstream as the pressure on downstream (pressure) side of the blade is higher than the ambient pressure. This is documented by the instantaneous pressure contours in figure 3b.

The pressure and viscous stresses over the blades yield thrust T and torque Q, which are non-dimensionalized as

$$K_T = \frac{T}{\rho n^2 D^4}, \qquad K_Q = \frac{Q}{\rho n^2 D^5}$$

where ρ is the fluid density, n is the propeller rotational speed in rev/s and D is the diameter of the propeller. Their values are seen to strongly depend on Reynolds number. The non-dimensional thrust K_T and torque K_Q are plotted in Fig. 4a and 4b as they change during the computation. The horizontal axes show time elapsed since the beginning of the computation in propeller revolutions. Note that after each change in Reynolds number, both thrust and torque quickly stabilize and then remain nearly constant with time. The low level of fluctuation in thrust and torque in

forward mode is in agreement with experiment. Also shown are the steady experimental values of thrust and torque coefficients measured in a 36 inch water tunnel by Jessup et al. (private communication), and in a tow-tank by Hecker & Remmers[11] and by Jessup et al. (private communication). Note that as the Reynolds number approaches the experimental value, both thrust and torque approach the experimental results. Also, the computed out-of-plane force (ie. the force orthogonal to the axis of propeller) in Fig. 4c is very small. Experimental and computed values of thrust and torque in forward operation are summarized in Table 1.

Table 1: Thrust and torque in forward operation (J = 0.889): experimental and computed results. All experimental data, including Hecker & Remmers, were kindly provided by Jessup (private communication) at different advance ratios.

Forward	J	K_T	K_Q
Tow-tank, Hecker & Remmers [13]	0.889	0.2113	0.04197
Tow-tank, Jessup (data 11/2004)	0.889	0.2011	0.04205
Water tunnel, Jessup (data 6/2005)	0.891	0.2099	0.04407
Computed result	0.889	0.21	0.041

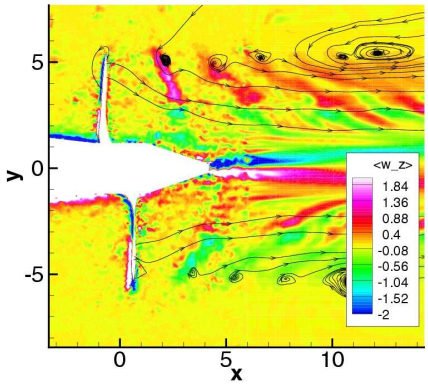

Figure 5: Vorticity contours and streamlines in frame of reference moving with upstream flow. Note the tip vortices and blade wakes. Computed results for forward operation J = 0.889, Re = 894,000 are averaged over 2.8 revolution in the propeller frame of reference.

A propeller blade is a finite twisted wing and therefore there is a trailing tip vortex starting at each blade. Due to propeller rotation, the vortices follow helical trajectories. Intersections of the helical vortices with the axial plane are visible in figure 5, which shows streamlines in a frame of reference moving with the upstream flow, and contours of z-component of vorticity. Figure 5 shows computed results for J=0.889 and Re=894,000 averaged over 2.8 revolutions. A similar plot is shown by the experimental study of Di Felice et al. for a different propeller[12] in Fig. 10 of their paper. The computed results show good qualitative agreement with Di Felice et al.'s results. The contours of vorticity reflect locations of the blade wakes. Notice, that as the wake gets further from the propeller, it is stretched. This is due to higher axial velocity closer to the axis. Also seen clearly is the hub vortex.

B. Crashback

Simulations were performed under crashback conditions at advance ratio J=-0.7 for which experimental data are available measured in a 36 inch water tunnel by Jessup et al.[2] and in a tow tank by Hecker & Remmers[13] and by Jessup (private communication). The computational grid was the same as that used in forward mode. The simulation was started with a uniform flow as the initial condition with velocity equal to the far field flow velocity. The Reynolds number was Re=1,200, and 336 time steps per revolution were used. After 12 propeller revolutions, the Reynolds number was increased to Re=12,000 and another 28 propeller revolutions were computed using 1680 time steps per revolution. Using the same time step, the Reynolds number was further increased to Re=120,000 for 3

revolutions and then finally to Re=480,000 for another 116 revolution. The last 100 revolutions were used to collect statistics. Note that the experiments of Jessup et al. (private communication) has shown that thrust does not depend on Reynolds number in range $4\times10^5 < Re < 9\times10^5$. We assume that not only thrust, but also torque and flow around propeller are similar in this range of Reynolds numbers, so that comparison with available experimental data can be made.

Crashback is fairly complex, as can be seen by comparing the forward mode in Fig. 3 to crashback in Fig. 6. Figure 6a shows streamlines and axial velocity contours in a plane along the propeller axis while Fig. 6b shows axial velocity contours in a plane perpendicular to the axis of propeller. There is a region of reversed flow close to the propeller in crashback (the blue and green region). This reversed flow interacts with ambient flow and creates a recirculation zone, which is often called a ring vortex. Figure 6b shows the resulting asymmetry of the solution in the various blade passages.

The flow in crashback is highly unsteady as is documented in Fig. 7, which shows pressure contours (normalized by ρU^2) and streamlines at two different times. As can be seen from the streamlines, an unsteady ring vortex is form as observed in experiments by Jiang[1]. The ring vortex move upstream and downstream and it tilts, which affects thrust, torque and out-of-plane forces on propeller. Figure 7a corresponds to higher absolute value of thrust whereas Fig. 7b corresponds to lower absolute value of thrust. This difference in thrust is obvious from the pressure contours – Fig. 7a shows higher pressure drop across the blades than Fig. 7b. Also note that the sign of the pressure difference on the blades in crashback is opposite than that in forward operation.

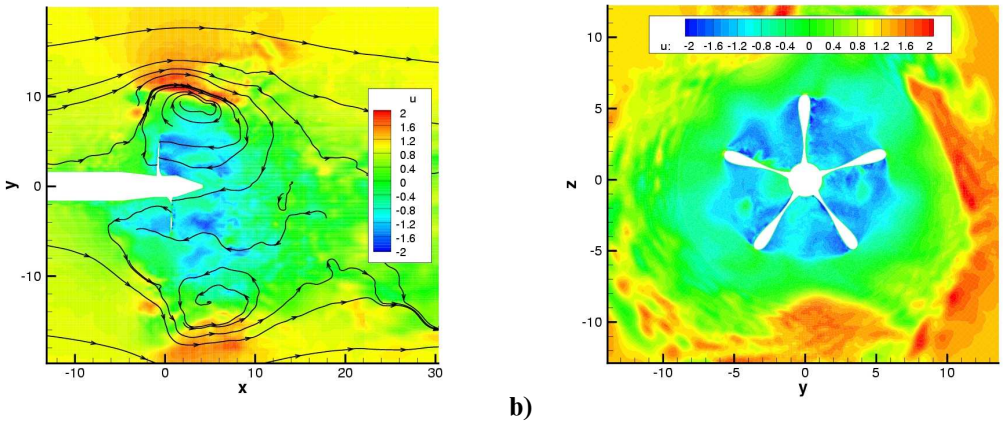

a) **b)**

Figure 6: Contours of axial velocity normalized by *U* and streamlines for crashback *J* = -0.7, *Re* = 480,000: (a) side view (b) axial view at *x / D = 0*.

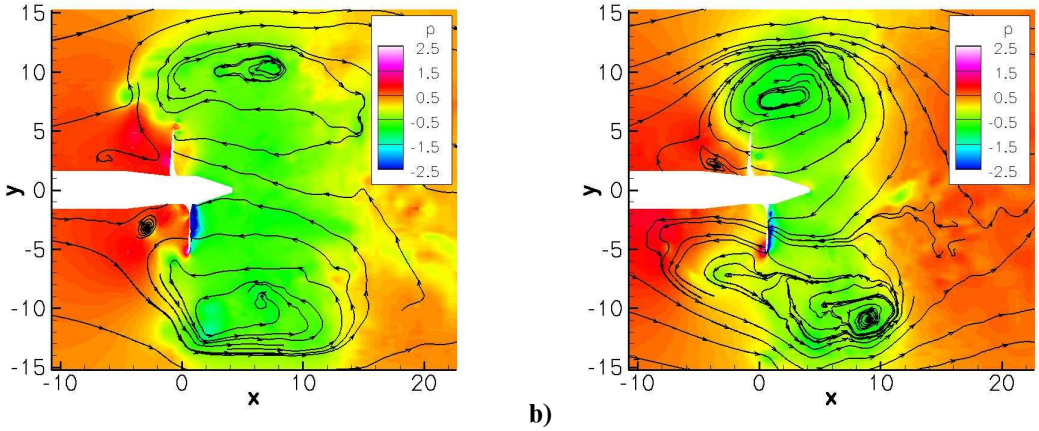

a) **b)**

Figure 7: Contours of axial velocity normalized by *U* and streamlines for crashback *J* = -0.7, *Re* = 480,000: (a) side view (b) axial view at *x / D = 0*.

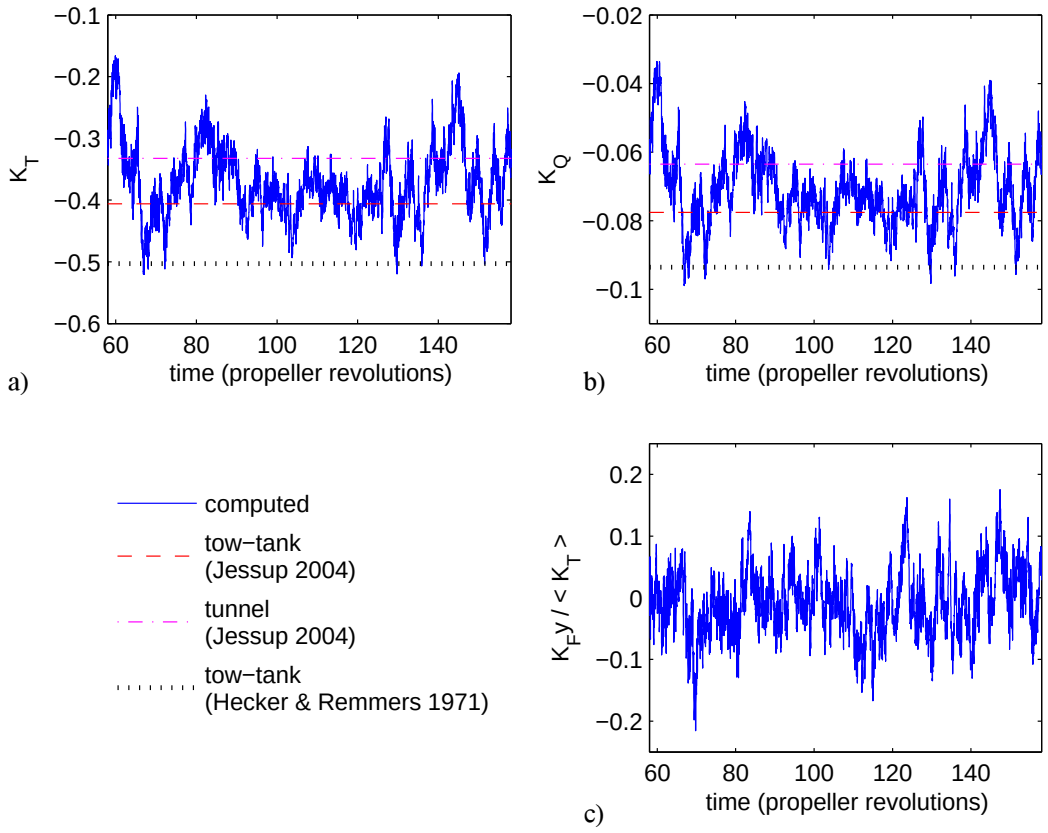

Figure 8: Illustration of unsteady loads in crashback (*J* = -0.7, *Re* = 480,000). Time history of non-dimensional (a) thrust K_T, (b) torque K_Q and (c) $K_F/<K_T>$. Here K_F denotes a component of force in a direction perpendicular to the propeller axis and fixed with respect to steady coordinates, $<K_T>$=-0.37 is the average thrust. All experimental data are from Table 2.

Table 2: Thrust and torque in crashback (J = -0.7): experimental data. All experimental data, including Hecker & Remmers, were kindly provided by Jessup (private communication) at different advance ratios.

Crashback	**J**	K_T	K_Q
Tow-tank, Hecker & Remmers [13]	-0.7	-0.5030	-0.09360
Tow-tank, Jessup (data 11/2004)	-0.7	-0.4062	-0.07777
Water tunnel, Jessup (data 9/2004)	-0.699	-0.3323	-0.06504
Computed result (averaged over 100 revolutions)	-0.7	-0.37	-0.071

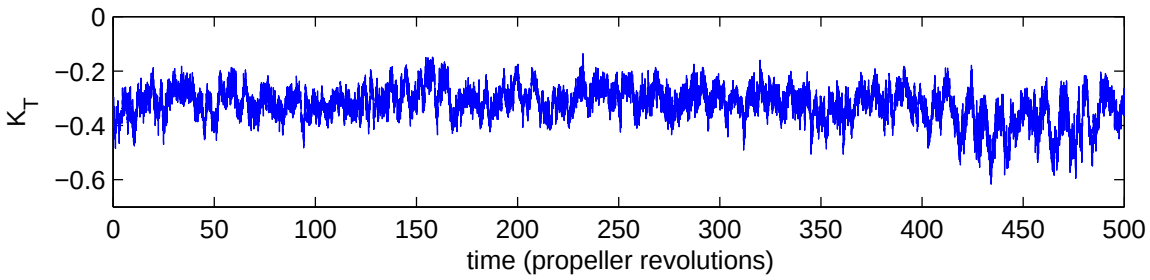

Figure 9: Evolution of non-dimensional thrust in crashback (J=-0.7) as measured in a water tunnel (provided by Jessup - private communication). Note irregularity on long timescale.

The asymmetry and unsteadiness of flow is reflected in the blade loads and hence also in thrust, torque and in out-of-plane forces. Figures 8a and 8b show the time history of computed non-dimensional thrust and torque, respectively. Also shown are the experimental values of average thrust and torque coefficients obtained by Jessup et al.[2] in a water tunnel, and Hecker & Remmers[11] and Jessup (private communication) in a tow tank. Note that both thrust and torque exhibit large irregular fluctuations with low frequency. The amplitude and timescale of these fluctuations is similar to fluctuations of thrust in Fig. 9, which shows data measured by Jessup et al. in a water tunnel. Thrust and torque also contain smaller amplitude oscillations with frequency 5 per revolution, which correspond to passage of individual blades of the five-bladed propeller. The evolution of computed out-of-plane force normalized by thrust is plotted in Fig. 8c. These are the forces perpendicular to the propeller axis. The magnitude and unsteadiness of out-of-plane forces in crashback is seen to be much larger than in forward operation due to high asymmetry and unsteadiness of the flow in crashback. It is in good agreement with experiment.

The computed mean values of thrust and torque are compared to experiment in Table 2. The water tunnel results show smaller absolute values of average thrust and torque than tow-tank results. Mean thrust and torque computed here lies between the water tunnel and the tow-tank results of Jessup et al.

Note that the thrust, torque and out-of-plane forces exhibit irregularities even on a long time scale, therefore longer computation would be necessary for precise statistics. Figure 9 illustrates these irregularities on an example of thrust as measured by Jessup et al. Notice e.g. that after 400 revolutions, the thrust achieves extreme negative values. The length of the computation in this paper is only for 100 revolutions. Longer computation is planned for the future.

Circumferentially averaged mean velocities and root-mean-square (RMS) of velocity fluctuations also show good agreement with experiment. The computed results were averaged circumferentially and in time over a period of 100 revolutions, and compared with corresponding experimental results of Jessup et al.[2] Figure 10a shows contours of computed axial velocity and streamlines, Fig. 10b shows experimental result. Note the reverse flow through the region where propeller blades operate. This reversed flow interacts with surrounding flow to create a ring vortex. The computed ring vortex is somewhat closer to the propeller than the ring vortex observed in experiment, but the computed axial velocity is in a good agreement with experiment. Figure 11 compares computed and measured velocity in the circumferential direction (the propeller rotates in negative circumferential direction). The computed and measured data show very good agreement upstream from propeller (upstream with respect to free-stream flow), but downstream of the propeller, where the circumferential velocity is smaller, the agreement is weaker. The recirculation zone might require higher resolution to get better agreement of circumferential velocity downstream, but as its amplitude is small, it probably would not effect prediction of propeller performance. The radial component of velocity in Fig. 12 shows very good agreement upstream of propeller. The computed radial velocity downstream of propeller drops faster than the measured radial velocity, which is consistent with location of the computed ring vortex slightly upstream of the ring vortex in experiment. Figure 13 compares root-mean-square fluctuation of velocity with experiment. Note that only resolved motions, not subgrid-scale fluctuations in LES are considered when RMS fluctuation of velocity is computed. Both graphs show high RMS fluctuation velocity in ring vortex region. A good agreement is achieved except in a small region near the tip of blade where experiment shows high RMS fluctuation velocity, but only small value is predicted. Overall, the circumferentially averaged velocity and RMS show encouraging agreement.

IV. Conclusions

LES was applied to the turbulent flow around a marine propeller in forward and crashback operation. The qualitative features and the values of thrust and torque for forward operation are in very good agreement with experiment. The crashback simulations show the presence of an unsteady ring vortex, and low frequency unsteadiness in the thrust and torque coefficients. The simulations also predict significantly higher levels of forces orthogonal to the axis of propeller, which would affect overall maneuverability. The results for thrust, torque and circumferentially averaged mean velocities and RMS of velocity fluctuation show reasonable agreement with experimental measurements.

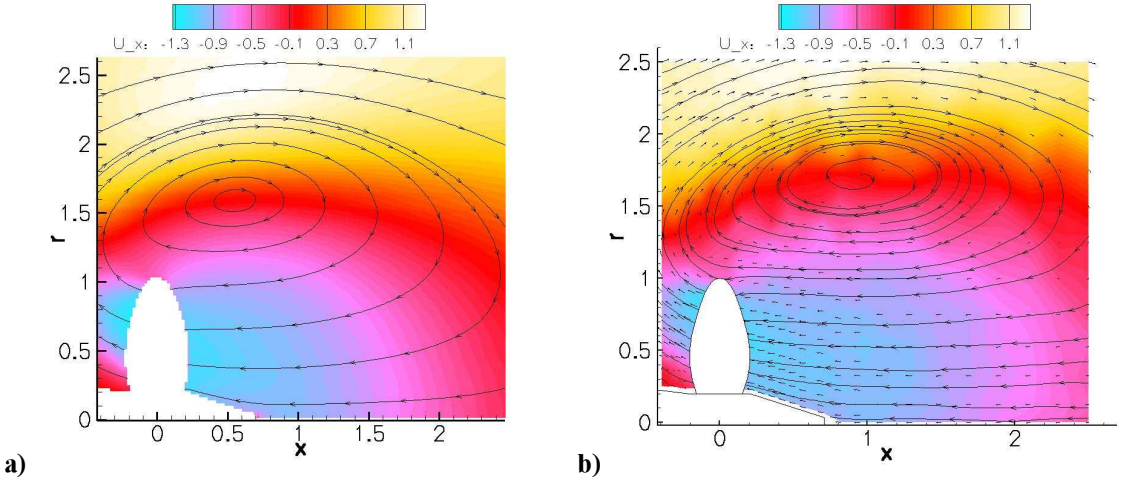

Figure 10: Axial velocity in crashback (J=-0.7) averaged circumferentially and in time normalized by free stream velocity: a) computed over 100 propeller revolutions at Re=480,000, b) measured by Jessup at al.[2] in water tunnel (Re=650,000).

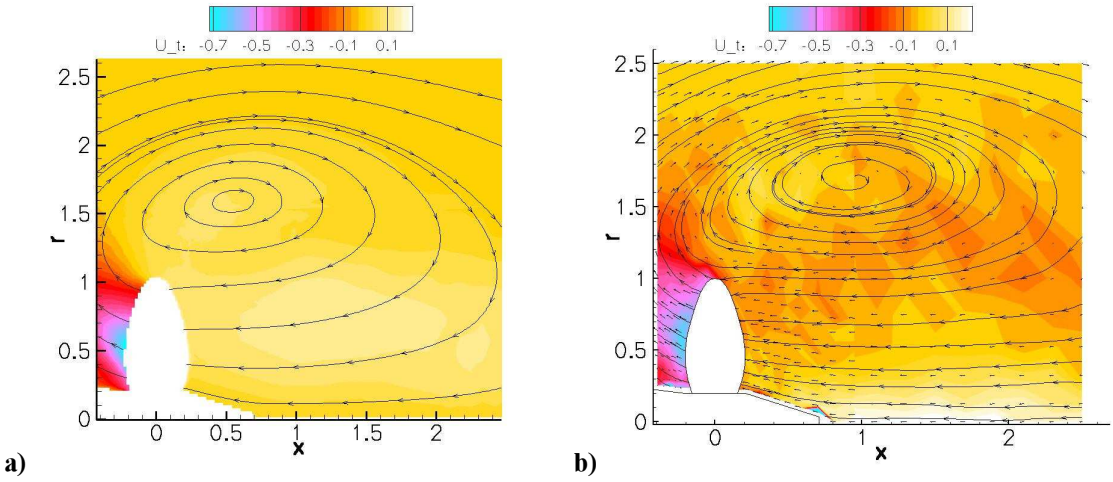

Figure 11: Tangential velocity in crashback (J=-0.7) averaged circumferentially and in time normalized by free stream velocity: a) computed over 100 propeller revolutions at Re=480,000, b) measured by Jessup at al. (private communication) in water tunnel (Re=650,000).

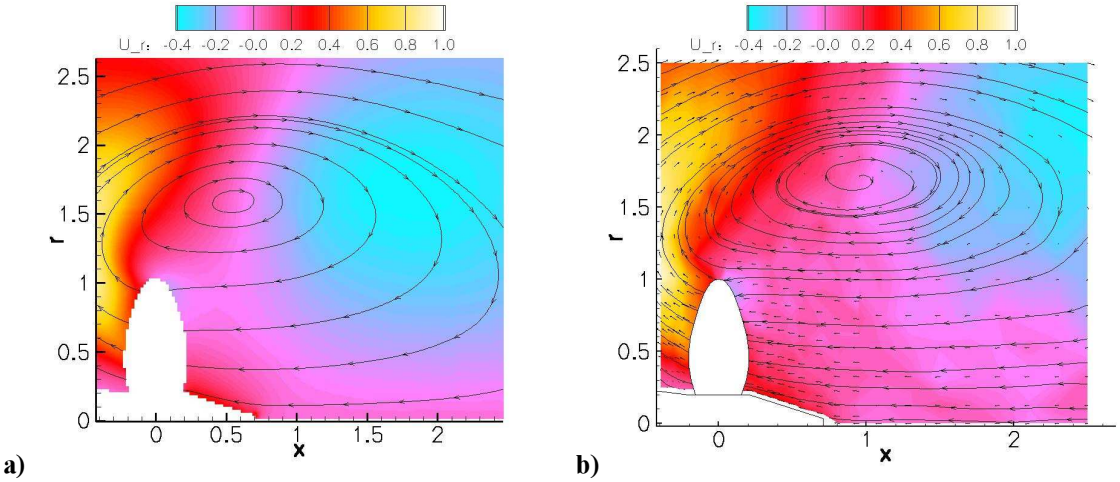

Figure 12: Radial velocity in crashback (J=-0.7) averaged circumferentially and in time normalized by free stream velocity: a) computed over 100 propeller revolutions at Re=480,000, b) measured by Jessup at al. (private communication) in water tunnel (Re=650,000).

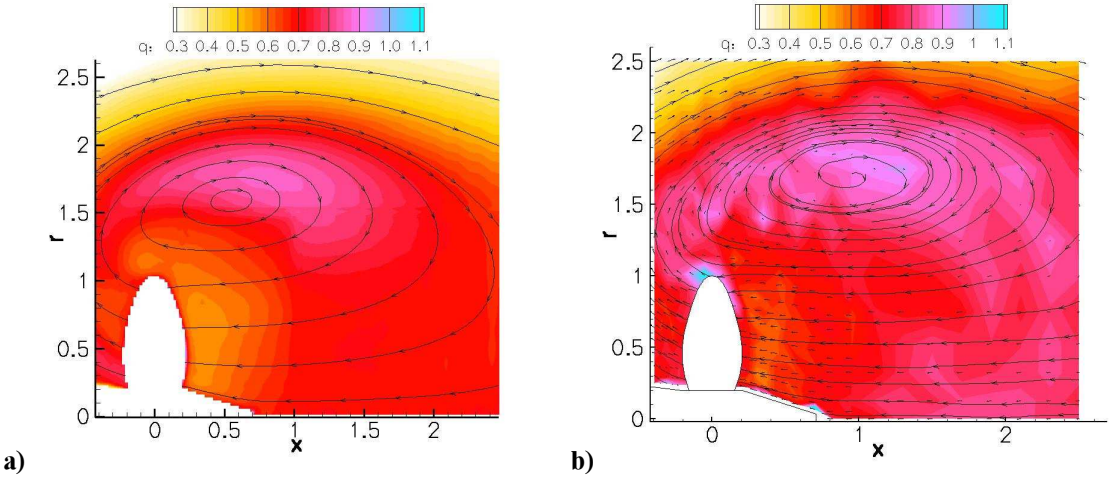

Figure 13: Root-mean-square fluctuation of velocity in crashback (J=-0.7) averaged circumferentially and in time normalized by free stream velocity: a) computed over 100 propeller revolutions at Re=480,000, b) measured by Jessup at al.[2] in water tunnel (Re=650,000).

Acknowledgements

This work was supported by the United States Office of Naval Research under ONR Grant N00014-02-1-0978 with Dr. Ki-Han Kim as technical monitor. Computing resources were provided by the San Diego Supercomputing Center, the National Center for Supercomputing Applications, and the Minnesota Supercomputing Institute. We are grateful to Dr. Stuart Jessup for providing us with experimental data, and for useful discussions.

References

[1]Jiang, C.-W., Dong, R. R., Liu, H.-L., Chang, M.-S., "24-inch Water Tunnel Flow Field Measurements During Propeller Crashback," *21st Symposium on Naval Hydrodynamics*, The National Academies Press, Washington, DC, 1997, pp. 136-146.

[2]Jessup, S., Chesnakas, C., Fry, D., Donnelly, M., Black, S., Park, J., "Propeller Performance at Extreme off Design Conditions," *25th Symposium on Naval Hydrodynamics*, The National Academies Press, Washington DC, 2004, pp. 270-292.

[3]Chen, B., Stern, F., "Computational Fluid Dynamics of Four-Quadrant Marine-Propulsor Flow," *Journal of Ship Research*, Vol. 43, No. 4, 1999, pp. 218-228.

[4]Davoudzadeh, F., Taylor, L. K., Zierke, W. C., Dreyer, J. J., McDonald, H., Whitfield, D. L., "Coupled Navier-Stokes and Equations of Motion Simulation of Submarine Maneuvers, Including Crashback," *Proceedings of the 1997 ASME Fluids Engineering Division Summer Meeting*, Vol. 2, ASME, New York, 1997.

[5]McDonald, H., Whitfield, D., "Self-Propelled Maneuvering Underwater Vehicles," *21st Symposium on Naval Hydrodynamics*, The National Academic Press, Washington, DC, 1996, pp. 478-489.

[6]Beddhu, M., Taylor, L. K., Whitfield, D. L., "Strong Conservative Form of the Incompressible Navier-Stokes Equations in a Rotating Frame with a Solution Procedure," *J. of Computational Physics*, Vol. 128, 1996, pp. 427-437.

[7]Majety, K. S., "Solutions to the Navier-Stokes Equations in a Non-Inertial Reference Frame," MS Thesis, Mississippi State University, 2003.

[8]Germano, M., Piomelli, U., Moin, P., Cabot, W. H., "A Dynamic Subgrid-Scale Eddy Viscosity Model," *Physics of Fluids A*, Vol. 3, No. 7, 1991, 1760-1765.

[9]Lilly, D. K., "A Proposed Modification of the Germano Subgrid-Scale Closure Method", *Phyics of Fluids A*, Vol. 4, No. 3, 1992, 633-635.

[10]Mahesh, K., Constantinescu, G., Moin, P, "A Numerical Method for Large-Eddy Simulation in Complex Geometries," *J. of Computational Physics*, Vol. 197, No. 1, 2004, 215-240.

[11]Hecker, R., Remmers, K, "Four Quadrant Open-Water Performance of Propellers 3710, 4024, 4086, 4381, 4382, 4383, 4384 and 4426," David Taylor Naval Ship Research and Development Center, report NSRADC 417-H01, 1971.

[12]Di Felice, F., Romano, G., Elefante, M., "Propeller wake analysis by means of PIV," *23rd Symposium on Naval Hydrodynamics*, The National Academic Press, Washington, DC, 2001, pp. 493-510.